polymers

MDPI

Article

Synthesis, Structural Characterization and Ligand-Enhanced Photo-Induced Color-Changing Behavior of Two Hydrogen-Bonded Ho(III)-Squarate Supramolecular Compounds

Chih-Chieh Wang [1,*], Szu-Yu Ke [1], Yun Feng [1], Mei-Lin Ho [1,*], Chung-Kai Chang [2], Yu-Chun Chuang [2] and Gene-Hsiang Lee [3]

[1] Department of Chemistry, Soochow University, Taipei 11102, Taiwan
[2] Instrumentation Center, National Taiwan University, Taipei 10617, Taiwan
[3] Materials Science Group, National Synchrotron Radiation Research Center, Hsinchu 30076, Taiwan
* Correspondence: ccwang@scu.edu.tw (C.-C.W.); meilin_ho@scu.edu.tw (M.-L.H.); Tel.: +886-228-819-471 (ext. 6828) (C.-C.W.)

Received: 12 July 2019; Accepted: 15 August 2019; Published: 19 August 2019

check for updates

Abstract: Two coordination polymers (CPs) with chemical formulas, $[Ho_2(C_4O_4)_2(C_2O_4)(H_2O)_8]\cdot 4H_2O$ (**1**) and $[Ho(C_4O_4)_{1.5}(H_2O)_3]$ (**2**), ($C_4O_4^{2-}$ = dianion of squaric acid, $C_2O_4^{2-}$ = oxalate), have been synthesized and their structures were determined by single-crystal X-ray diffractometer (XRD). In compound **1**, the coordination environment of Ho(III) ion is eight-coordinate bonded to eight oxygen atoms from two squarate, one oxalate ligands and four water molecules. The squarates and oxalates both act as bridging ligands with $\mu_{1,2}$-*bis*-monodentate and *bis*-chelating coordination modes, respectively, connecting the Ho(III) ions to form a one-dimensional (1D) ladder-like framework. Adjacent ladders are interlinked via O–H···O hydrogen bonding interaction to form a hydrogen-bonded two-dimensional (2D) layered framework and then arranged orderly in an AAA manner to construct its three-dimensional (3D) supramolecular architecture. In compound **2**, the coordination geometry of Ho(III) is square-antiprismatic eight coordinate bonded to eight oxygen atoms from five squarate ligands and three water molecules. The squarates act as bridging ligands with two coordination modes, $\mu_{1,2,3}$-*tris*monodentate and $\mu_{1,2}$-*bis*-monodentate, connecting the Ho(III) ions to form a 2D bi-layered framework. Adjacent 2D frameworks are then parallel stacked in an AAA manner to construct its 3D supramolecular architecture. Hydrogen bonding interactions between the squarate ligands and coordinated water molecules in **1** and **2** both play important roles on the construction of their 3D supramolecular assembly. Compounds **1** and **2** both show remarkable ligand-enhanced photo-induced color-changing behavior, with their pink crystals immediately turning to yellow crystals under UV light illumination.

Keywords: coordination polymer; metal-organic framework; hydrogen bond; supramolecular architecture; color change

---

1. Introduction

Lanthanide metal-organic frameworks (LnMOFs) have received much attention, not only for their fascinating structural variety, but also for their potential applications of MOFs like porosity for gas storage [1–9], their specific characteristics arising from 4f electrons for luminescence [10–22]. The inherent character of lanthanide ions with high affinity for oxygen atoms and high coordination numbers, result in the formation of a number of MOFs with flexible coordination geometry and various structural dimensionality from multi-carboxylate ligands [13–29]. The squarate, $C_4O_4^{2-}$, has been widely used as a polyfunctional ligand, including (1) acts as a bridging ligand with various coordination modes (μ_2 to μ_6 bridges shown in Scheme 1) to build up many coordination polymers with novel extended networks, including 1D chain, 2D layer, 3D cube- and cage-like frameworks and so forth and (2) behaviors as hydrogen bond donor, acceptor or π−π constructor for the assembly of extended supramolecular architecture [30–63]. In the previous investigation, several 2D and 3D LnMOFs constructed via the bridges of lanthanide and squarate ligand with various coordination modes have been synthesized under hydrothermal or solvothermal conditions [64–70]. Their thermal behavior, magnetic property and photo-luminescence spectra of 2D and 3D LnMOFs have also been studied. With our continuous effort on the study of metal-squarate coordination polymers (CPs) [58–63], we report here the synthesis, structural characterization, thermal stability and light-induced color-changing behavior of two Ho(III)-squarate hydrogen-bonded supramolecular networks, $[Ho_2(C_2O_4)(C_4O_4)_2(H_2O)_8]·4H_2O$ (**1**) and $[Ho(C_4O_4)_{1.5}(H_2O)_3]$ (**2**), ($C_4O_4^{2-}$ = dianion of squaric acid, $C_2O_4^{2-}$ = dianion of oxalic acid), in which the squarate acts as the bridging ligands with $\mu_{1,2}$-coordination mode (Scheme 1b) for **1** and combined $\mu_{1,2}$-plus $\mu_{1,2,3}$-coordination modes (Scheme 1b,c) for 2 to build up 1D ladder-like CP and 2D bi-layered MOF, respectively.

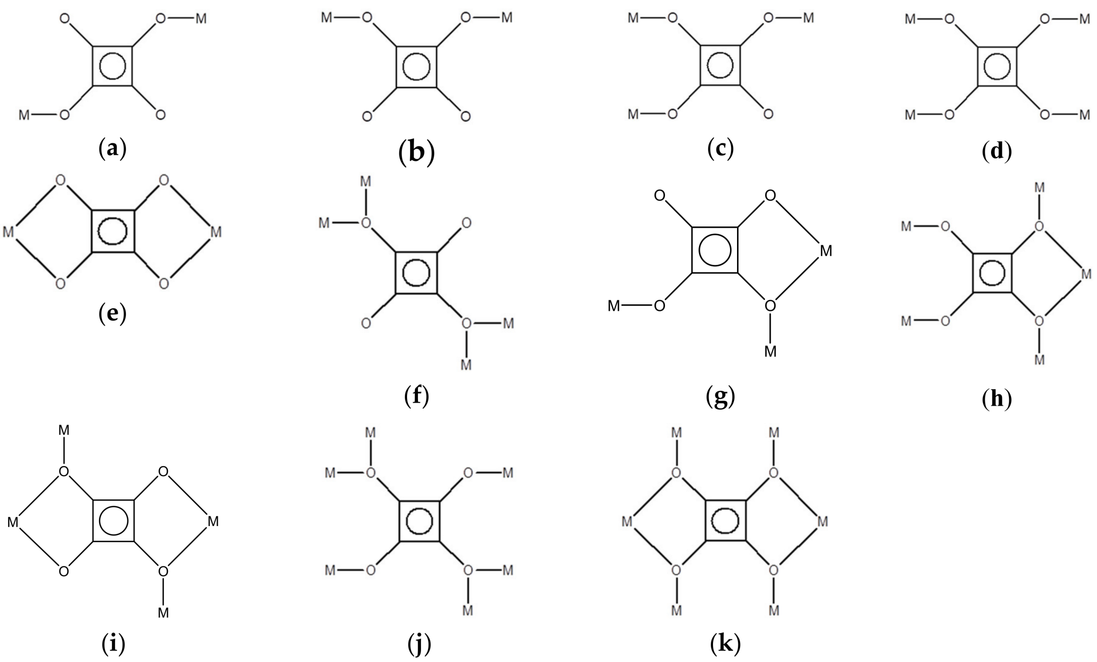

Scheme 1. Coordination modes of squarate on the construction of extended 1D, 2D or 3D networks: (**a**) $\mu_{1,3}$-*bis*-monodentate, (**b**) $\mu_{1,2}$-*bis*-monodentate, (**c**) $\mu_{1,2,3}$-*tris*-monodentate, (**d**) $\mu_{1,2,3,4}$-*tetrakis*-monodentate, (**e**) bidentate μ_2−, (**f**) monodentate μ_4−, (**g**) bidentate/monodentate μ_3−, (**h**) bidentate/monodentate μ_5−, (**i**) bidentate/monodentate μ_4−, (**j**) monodentate μ_6−, (**k**) bidentate/monodentate μ_6−.

2. Materials and Methods

2.1. Materials and General Methods

All the reagents (Sigma-Aldrich Inc., Taipei, Taiwan) were purchased commercially and used without further purification. Elementary microanalyses (EA) (C, H and N) were performed using a Perkin-Elmer 2400 elemental analyzer (PerkinElmer, Taipei, Taiwan). FTIR spectra (500–4000 cm^{-1}) were recorded from KBr pellets with a Nicolet Fourier Transform IR, MAGNA-IR 500 spectrometer (ThermoFisherScientific, Waltham, MA, USA). Thermal analysis (TGA) was carried out using a Perkin-Elmer 7 Series/UNIX TGA7 analyzer (PerkinElmer, Taipei, Taiwan) under a nitrogen atmosphere in the temperature range of 25 °C–700 °C with a ramp rate of 5 °C/min.

*2.2. Synthesis of [$Ho_2(C_2O_4)(C_4O_4)_2(H_2O)_8$]·$4H_2O$ (**1**) and [$Ho(C_4O_4)_{1.5}(H_2O)_3$]·H_2O (**2**)*

Method 1: Squaric acid ($H_2C_4O_4$, 8.6 mg, 0.075 mmol) was dissolved in 3 mL mixed solvents of distilled water and EtOH (1:1, *v/v*) and then added into the solution of $Ho(NO_3)_3·5H_2O$ (22.1 mg, 0.05 mmol) and 4,4′-bipyridyl-N,N′-dioxide hydrate (bpno, 9.4 mg, 0.05mmol) in 6 mL mixed solvents of distilled water and EtOH at room temperature to give a colorless solution. Light-pink needle-like and block-like crystals of **1** and **2**, respectively, were obtained after several weeks in 2.69% and 47.3% yields. The resulting crystals were collected by filtration, washed several times with distilled water and dried in air.

Method 2: The synthetic procedure was similar to method 1 except $Na_2C_2O_4$ was added into the reaction solution, with the molar ratios of squaric acid ($H_2C_4O_4$, 8.5 mg, 0.075 mmol), $Ho(NO_3)_3·5H_2O$ (44.1 mg, 0.1 mmol), 4,4′-bipyridyl-N,N′-dioxide hydrate (bpno, 9.4 mg, 0.05mmol) and $Na_2C_2O_4$ (10.1 mg, 0.075 mmol) in 12 mL mixed solvents of distilled water and EtOH at room temperature. Only light-pink needle-like crystals of **1** were obtained after four weeks in 66.4% yields. The resulting crystals were collected by filtration, washed several times with distilled water and dried in air.

Anal. Calcd for $HoC_5H_{12}O_{12}$ (**1**) (Mw=429.07): C 14.00, H 2.82. Found: C 13.92, H 2.81. IR (KBr pellet): ν = 3340 (s), 1681 (s), 1607 (s), 1536 (s), 1477 (vs), 1317 (m), 1098 (m), 869 (m), 830 (m), 659 (m), 537 (m), 494 (m) cm^{-1}. Anal. Calcd for $HoC_6H_8O_{10}$ (**2**) (Mw = 405.05): C 17.79, H 1.99 Found: C 17.68, H 1.85. IR (KBr pellet): 3420 (s), 3101 (m), 1605 (s), 1509 (vs), 1097 (m), 858 (m), 741 (m), 671 (m), 645 (m) cm^{-1}.

2.3. Crystallographic Data Collection and Refinements

Single crystals of **1** and **2** suitable for X-ray structural analyses were selected and their crystallographic data were collected at 150 K and 250 K, respectively, on a Siemens SMART CCD diffractometer using Mo radiation (λ = 0.71073 Å) in the ω scan mode. Cell parameters were retrieved using SMART [71] software and the detector frames were integrated by use of program SAINT [72]. Data reduction was performed by use of program SAINT [73] and corrected for Lorentz and polarization effects. The empirical absorption corrections were performed using the SADABS [73] program. Both the structures were solved by direct method and refined by full-matrix, least-squares procedures using the SHELXTL-PC V 5.03 software [74]. All non-hydrogen atoms were refined subjected to anisotropic refinements. The hydrogen atoms of the coordinated and solvated water molecules were located in the Difference Fourier map with the corresponding positions and isotropic displacement parameters being refined. The final full-matrix, least-squares refinement on F^2 was applied for all observed reflections (I > 2σ(I)). Details of crystallographic data, data collections and structure refinements **1** and **2** are summarized in Table 1. CCDC 1940248 and 1940249 for **1** and **2**, respectively.

Table 1. Crystal data and refinement details of compounds **1** and **2**.

Compound	1	2
empirical formula	$C_{10}H_{24}Ho_2O_{24}$	$C_6H_8Ho_1O_{10}$
formula mass (g mol^{-1})	858.15	405.05
crystal system	Triclinic	Monoclinic
space group	*P*-1	$P2_1/c$
***a* (Å)**	7.2463(8)	11.8844(11)
***b* (Å)**	7.4084(8)	8.1321(7)
***c* (Å)**	12.6393(14)	9.9939(9)
α (deg)	96.599(2)	90.00
β (deg)	93.691(2)	96.097(2)
γ (deg)	116.651(2)	90.00
***V* (Å^3)**	597.26(11)	960.40(15)
Z	2	4

Table 1. *Cont.*

Compound	1	2
T (K)	150(2)	250(2)
D_{calcd} **(g cm^{-3})**	2.386	2.801
μ (mm^{-1})	6.682	8.288
θ range (deg)	1.64–27.5	1.72–27.5
total no. of data collected	7686	6229
no. of unique data	2733	2215
no. of obsd data (I > 2 σ (I))	2570	2037
R_{int}	0.0514	0.0424
refine params	163	181
R_1, wR_2 [1] **(I > 2 σ (I))**	0.0430, 0.1089	0.0391, 0.0926
R_1, wR_2 [1] **(all data)**	0.0463, 0.1103	0.0424, 0.0940
GOF [2]	1.216	1.296

[1] $R_1 = \Sigma||F_o - F_c||/\Sigma|F_o|$; $wR_2(F^2) = [\Sigma w|F_o{}^2 - F_c{}^2|^2/\Sigma w(F_o{}^4)]^{1/2}$. [2] $GOF = \{\Sigma[w|F_o{}^2 - F_c{}^2|^2]/(n-p)\}^{1/2}$.

2.4. In Situ Powder X-ray Diffraction

The powder X-ray diffraction patterns of **1** and **2** were measured at the BL01C2 in National Synchrotron Radiation Research Center (NSRRC). The wavelength of the incident X-rays was 1.0332 Å (12.0 keV) and diffraction signals were recorded with a Mar345 imaging-plate detector. The powder sample was packed into a 0.3 mm diameter glass capillary. The diffraction geometry was calibrated by NIST standard reference material, lanthanum hexaboride (SRM660b). The one-dimensional diffraction pattern was converted with GSAS-II program [75].

2.5. Spectral Measurement

UV-vis diffusive reflectance spectra for compounds **1** and **2** were obtained with a HITACHI U-3900H spectrophotometer (Hitachi High Technologies America Inc., Schaumburg, IL, USA) equipped with an integrating sphere accessory (Al_2O_3 was used as a reference) [76].

3. Results and Discussion

3.1. Syntheses and Characterization of Compounds 1 and 2

Compounds **1**, $[Ho(C_2O_4)_{0.5}(C_4O_4)(H_2O)_4]\cdot 2(H_2O)$ and **2**, $[Ho(C_4O_4)_{1.5}(H_2O)_3]$, were synthesized by direct mixing of $Ho(NO_3)_3\cdot 5H_2O$, squaric acid ($H_2C_4O_4$) and 4,4′-bipyridyl-N,N′-dioxide (bpno) in the mixed solvents of distilled water and EtOH at room temperature (method 1) as shown in Scheme 2. In addition, compound **1** can also be obtained by the direct mixing of $Ho(NO_3)_3\cdot 5H_2O$, $H_2C_4O_4$, bpno and $Na_2C_2O_4$ in the mixed solvents of distilled water and EtOH (method 2). The yields of **1** are increasing from 2.69% to 66% but the crystals quality is not as good as those obtained by method 1. The bpno may act as a base for the deprotonation of the squaric acid. In the absence of bpno, compounds **1** and **2** were not produced during the reaction. In method 1, the oxalate ligand was obtained via the in-situ synthesis from the squarate ligand, indicating a slow release of oxalate from the squarate could be helpful for the formation of compound **1**. However, the formation mechanism of oxalate is not clear and may be through an in situ oxidation ring-opening reaction of squarate. This type of ring opening oxidation reaction has been proposed previously [77–79]. The most relevant IR features are those related to the bridging oxalate and squarate ligands. Strong bands are found centered at around 1681, 1607, 1536, 1477 and 1605, 1509 cm^{-1} for **1** and **2**, respectively, which are attributed to the vibration modes of the C=O and mixtures of C–O and C−C stretching motions. They are in agreement with the characteristic of the oxalate and $(CO)_n{}^{2-}$ salts [80]. Additional broad peaks for **1** and **2** appear in the region of 3100–3500 cm^{-1}, corresponding to the stretching vibration of ν(O−H) from water molecules.

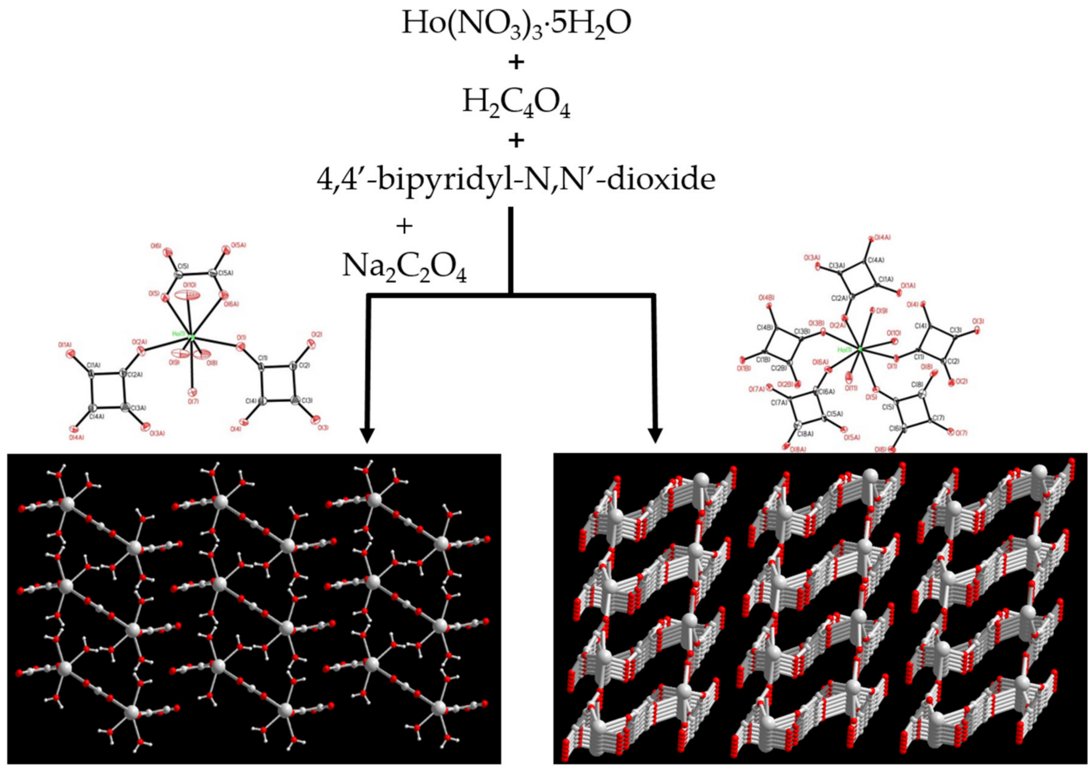

$[Ho(C_2O_4)_{0.5}(C_4O_4)(H_2O)_4] \cdot 2(H_2O)$ (**1**) $[Ho(C_4O_4)_{1.5}(H_2O)_3]$ (**2**)

Scheme 2. Synthetic representation of compounds **1** and **2** (red for O atom, and gray-white for Ho and C atoms).

3.2. Structure Description of $\{[Ho(C_2O_4)_{0.5}(C_4O_4)(H_2O)_4] \cdot 2H_2O\}_n$ (**1**)

The molecular structure of **1**, shown in Figure 1a, reveals that the Ho(III) ion is eight coordinate bonded with two oxygen donors from two squarate ($C_4O_4^{2-}$) ligands, two oxygen donors from one oxalate ($C_2O_4^{2-}$) ligand and four water molecules, with Ho(III)–O distances in the range of 2.314(6)–2.470(6). The related bond distances and angles around the Ho(III) ion are listed in Table 2. The $C_4O_4^{2-}$ acts as a bridging ligand with $\mu_{1,2}$-*bis*-monodentate coordination mode (Scheme 1b) connecting the Ho(III) ions to form a one-dimensional (1D) linear chain. Two linear chains are interlinked via the bridges of the Ho(III) ions and $C_2O_4^{2-}$ ligand with *bis*-chelating coordination mode, forming a 1D ladder-like CP (Figure 1b). Intra-ladder O−H···O type hydrogen bonds between the coordinated water molecules and uncoordinated oxygen of $C_4O_4^{2-}$ provide extra energy on the stabilization of these 1D CPs. The Ho···Ho separations bridged by the $C_4O_4^{2-}$ and $C_2O_4^{2-}$ ligands are 7.696(1) and 6.372(5) Å, respectively. It is worth to note that hydrogen bonding interaction in **1** play an important role on the extension of 1D ladder-like chains to 2D layered networks and then a 3D supramolecular architecture, as shown in Figure 1c,d. Firstly, adjacent 1D ladder-like polymeric chains are mutually interlinked via two inter-ladder O−H···O type hydrogen bonds between the coordinated water molecules (O(8) and O(9)) and uncoordinated oxygen atoms (O(3) and O(4)) of $C_4O_4^{2-}$ ligands, with O···O distance of 2.761(10) and 2.675(10) Å, respectively, extended to a two-dimensional (2D) hydrogen-bonded layered network (Figure 1c). Adjacent 2D hydrogen-bonded layers are arrayed in an orderly AAA stacking manner and then extended to its 3D supramolecular network (Figure 1d,e) via the intermolecular O−H···O type hydrogen bonds among the coordinated water molecules and the oxygen atoms of carbonyl groups of $C_4O_4^{2-}$ and $C_2O_4^{2-}$ ligands (yellow dashed lines shown in Figure 1d), with the O···O distance in the range of 2.677(10) ~ 2.825(10) Å. The 1D hydrophilic pores surrounded by squarate and oxalate ligands are generated with the pore size of 6.37 × 7.70 Å, as viewing along *a* axis (Figure 1e). Two guest water molecules (O(11) and O(12)) are intercalated into the 1D hydrophilic pores in the 3D supramolecular network (Figure 1e) and further stabilized via four O−H···O type hydrogen bonds between the oxygen atoms of $C_4O_4^{2-}$ and $C_2O_4^{2-}$ ligands in 1D polymeric chains and the guest water molecules. The related parameters of hydrogen bonds in **1** are listed in Table 3.

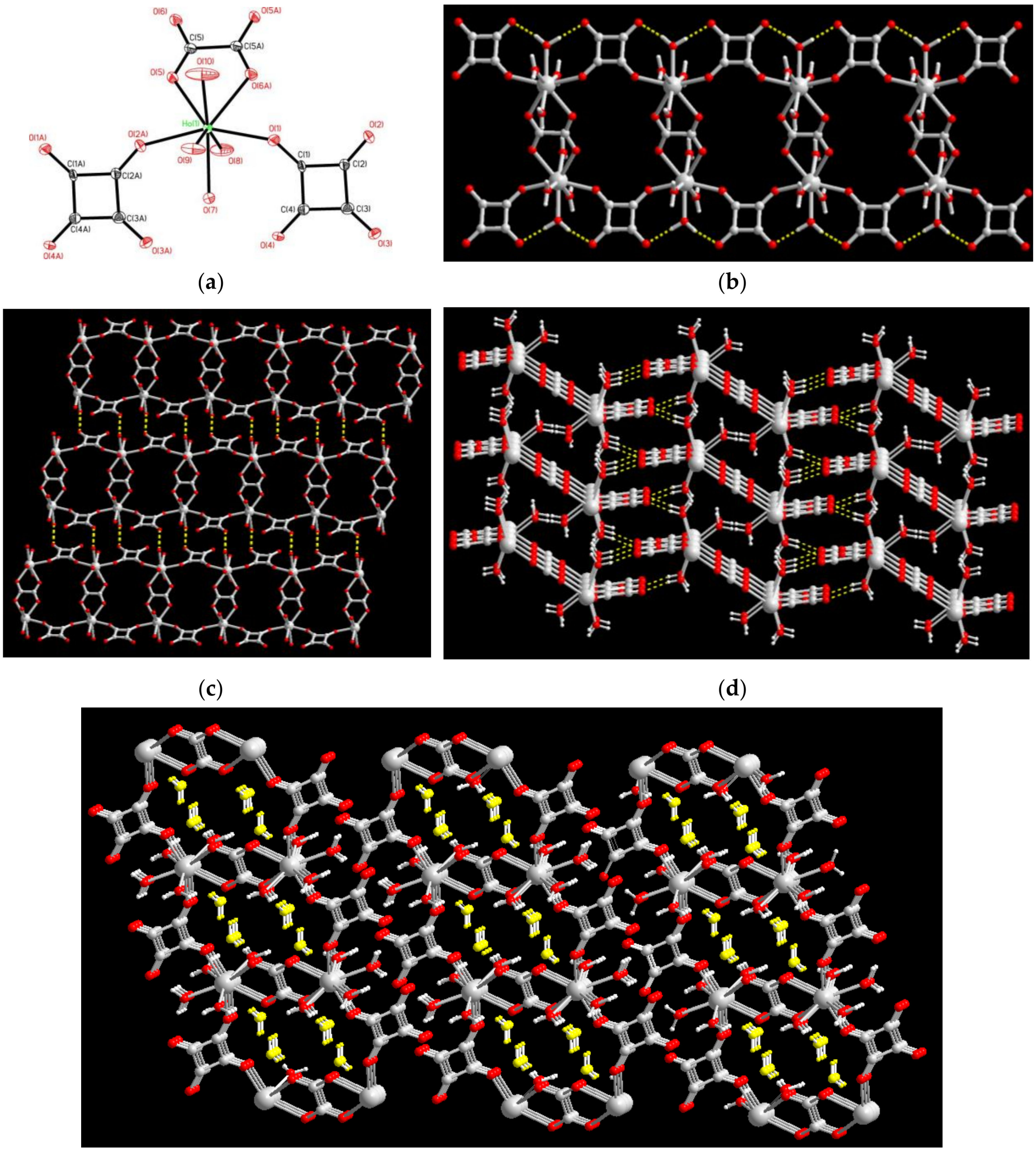

(e)

Figure 1. (**a**) Coordination environments of Ho(III) ion in **1** with atom labelling scheme (ORTEP drawing, 30% thermal ellipsoids). The guest water molecules and H atoms are omitted for clarity. (**b**) The 1D ladder-like framework constructed *via* the bridges of Ho(III) ions and $C_2O_4^{2-}$, $C_4O_4^{2-}$ ligands. (**c**) The 2D layered framework constructed via inter-ladder O−H···O hydrogen bonds (yellow dashed lines) between the squarate ligands and coordinated water molecules. (**d**) The 3D supramolecular assembly of **1** via the assembly of 1D ladder-like Chains. (Yellow dashed lines for inter-ladder O−H···O hydrogen bonds) (**e**) The 3D supramolecular assembly of **1** viewing along the *a* axis showing the guest water molecules (yellow color) intercalated into the 1D pores. (red for O atom, and gray-white for Ho and C atoms; yellow color for water molecules; yellow dashed lines for O−H···O hydrogen bonds).

Table 2. Bond lengths (Å) and angles (°) around Ho(III) ion in **1** [1].

Ho(1)–O(1)	**2.314(6)**	**Ho(1)–O(2)$_i$**	**2.317(6)**
Ho(1)–O(10)	2.319(7)	Ho(1)–O(8)	2.300(7)
Ho(1)–O(7)	2.326(6)	Ho(1)–O(9)	2.343(7)
Ho(1)–O(5)	2.431(6)	Ho(1)–O(6)$_{ii}$	2.470(6)
O(1)–Ho(1)–O(2)$_i$	153.3(2)	O(1)–Ho(1)–O(10)	92.0(3)
O(2)$_i$–Ho(1)–O(10)	100.3(3)	O(1)–Ho(1)–O(8)	90.3(3)
O(2)$_i$–Ho(1)–O(8)	91.9(3)	O(10)–Ho(1)–O(8)	147.2(3)
O(1)–Ho(1)–O(7)	78.8(2)	O(2)–Ho(1)–O(7)	76.5(2)
O(10)–Ho(1)–O(7)	140.2(3)	O(8)–Ho(1)–O(7)	72.2(2)
O(1)–Ho(1)–O(9)	83.6(3)	O(2)$_i$–Ho(1)–O(9)	79.4(3)
O(10)–Ho(1)–O(9)	67.9(3)	O(8)–Ho(1)–O(9)	144.8(2)
O(7)–Ho(1)–O(9)	72.6(2)	O(1)–Ho(1)–O(5)	136.0(2)
O(2)$_i$–Ho(1)–O(5)	70.3(2)	O(10)–Ho(1)–O(5)	76.5(3)
O(8)–Ho(1)–O(5)	79.3(2)	O(7)–Ho(1)–O(5)	135.0(2)
O(9)–Ho(1)–O(5)	127.5(3)	O(1)–Ho(1)–O(6)$_{ii}$	70.9(2)
O(2)$_i$–Ho(1)–O(6)$_{ii}$	135.3(2)	O(10)–Ho(1)–O(6)$_{ii}$	73.2(3)
O(8)–Ho(1)–O(6)$_{ii}$	76.7(2)	O(7)–Ho(1)–O(6)$_{ii}$	136.0(2)
O(9)–Ho(1)–O(6)$_{ii}$	132.2(2)	O(5)–Ho(1)–O(6)$_{ii}$	65.1(2)

[1] Symmetry transformations used to generate equivalent atoms: i = x−1, y−1, z; ii = −x, −y, −z+1.

Table 3. The O–H···O hydrogen bonds for **1** [1].

D–H···A	**D–H (Å)**	**H···A (Å)**	**D···A (Å)**	**∠ D–H···A (°)**
O(7)–H(7A)···O(4)	0.852(6)	1.778(6)	2.627(10)	174.3(5)
O(7)–H(7B)···O(3)$_i$	0.851(6)	1.812(6)	2.654(10)	169.8(6)
O(8)–H(8A)···O(3)$_{ii}$	0.853(6)	1.918(6)	2.761(10)	169.6(6)
O(8)–H(8B)···O(11)	0.850(6)	1.915(6)	2.816(10)	170.2(6)
O(9)–H(9A)···O(4)$_{iii}$	0.851(6)	1.832(6)	2.675(10)	170.2(6)
O(9)–H(9B)···O(12)$_{iv}$	0.849(6)	1.887(6)	2.706(10)	161.7(6)
O(10)–H(10A)···O(12)$_{)iv}$	0.849(6)	1.831(6)	2.678(10)	174.5(6)
O(10)–H(10B)···O(11)$_v$	0.849(6)	1.829(6)	2.677(10)	175.6(6)
O(11)–H(11A)···O(2)$_{vi}$	0.848(6)	2.058(6)	2.772(10)	141.4(6)
O(11)–H(11B)···O(1)$_{vi}$	0.846(6)	1.998(6)	2.785(10)	154.3(6)
O(12)–H(12A)···O(6)$_v$	0.846(6)	1.946(6)	2.782(10)	169.2(6)
O(12)–H(12B)···O(5)$_{vii}$	0.852(6)	1.997(6)	2.825(10)	163.6(6)

[1] Symmetry transformations used to generate equivalent atoms: i = x−1, y−1, z; ii = −x+1, −y+1, −z+2; iii = −x, −y+2, −z+2; iv = x−1, y, z; v = −x, −y+1, −z+1; vi = x, y−1, z; viii = x+1, y+1, z.

*3.3. Structure Description of [Ho(C$_4$O$_4$)$_{1.5}$(H$_2$O)$_3$]$_n$ (**2**)*

The molecular structure of **2**, shown in Figure 2a, reveals that the Ho(III) ion is eight coordinate in a square antiprismatic geometry bonded with three oxygen donors from three $\mu_{1,2,3}$-squarates, two oxygen donors from two $\mu_{1,2}$-squarates and three water molecules with Ho(III)–O distances in the range of 2.305(5)–2.415(5). The related bond distances and angles around the Ho(III) ions are listed in Table 4. The $C_4O_4^{2-}$ acts as a bridging ligand with two types of coordination modes, $\mu_{1,2,3}$-*tris*-monodentate (Scheme 1c) and $\mu_{1,2}$-*bis*-monodentate (Scheme 1b) coordination modes, in which the first one connect the Ho(III) centers to form a two-dimensional (2D) layered framework (Figure 2b, left). Two layers are mutually interlinked via the bridges of the Ho(III) ions and disorder $\mu_{1,2}$-*bis*-monodentate $C_4O_4^{2-}$ (Figure 2b, right), forming a 2D bi-layered MOF (Figure 2b, center). The Ho···Ho separations bridged by the $\mu_{1,2,3}$-*tris*-monodentate $C_4O_4^{2-}$ ligand are 6.399(1), 6.486(1) and 8.132(1) Å and bridged by the $\mu_{1,2}$-*bis*-monodentate $C_4O_4^{2-}$ ligand is 6.508(4) Å, respectively. Similar to **1**, hydrogen bonding interaction in **2** also play an important role on the extension of 2D bi-layered MOFs to a 3D supramolecular architecture, as shown in Figure 2c. Adjacent 2D bi-layered MOFs are arrayed in an orderly AAA stacking manner and extended to its 3D supramolecular network (Figure 2c,d) via the intermolecular O–H···O type hydrogen bonds among the coordinated water molecules and the oxygen atoms of $C_4O_4^{2-}$ (yellow dashed lines in Figure 2c,d) with the O···O distance in the range of 2.668(5)–2.914(5) Å. The related parameters of hydrogen bonds are listed in Table 5.

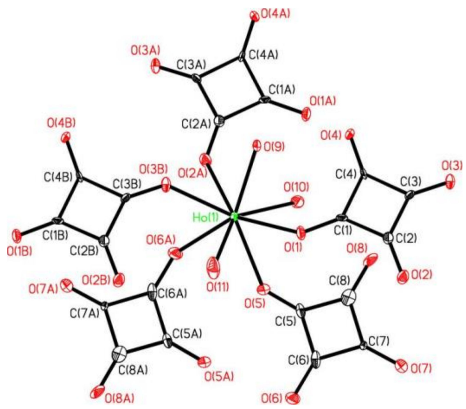

(a)

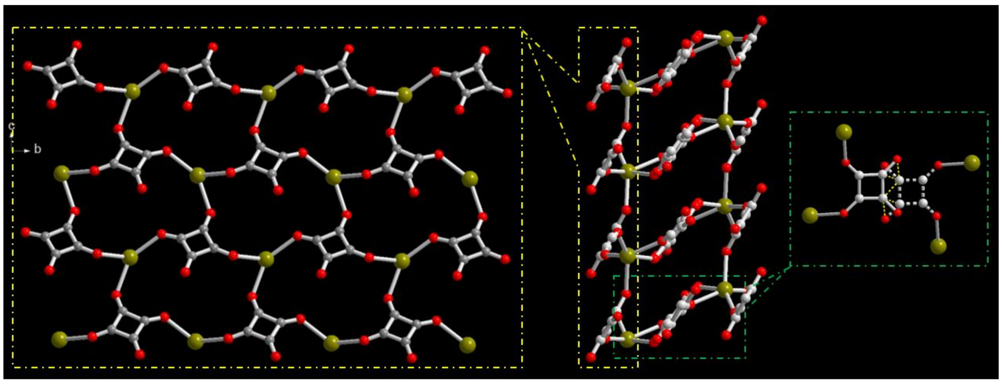

(b)

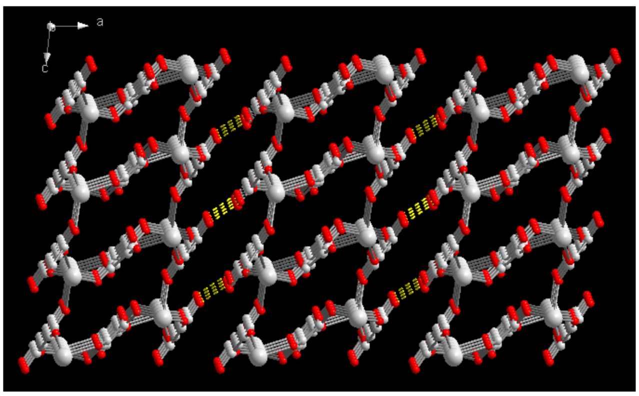

(**c**)

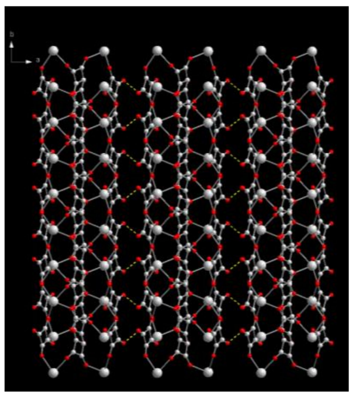

(**d**)

Figure 2. (**a**) A square antiprismatic geometry of Ho(III) ion in **2** with atom labelling scheme (ORTEP drawing, 30% thermal ellipsoids) The H atoms are omitted for clarity. (**b**) Left: The 2D layered framework via the bridges of Ho(III) ions and $\mu_{1,2,3}$-$C_4O_4^{2-}$. Middle: The 2D bi-layers MOFs constructed via the bridges of Ho(III) and $\mu_{1,2,3}$- and $\mu_{1,2}$-$C_4O_4^{2-}$. Right: The bridges of Ho(III) and disorder $\mu_{1,2}$-$C_4O_4^{2-}$. (red for O atom, gray-white for C atom and green-gray for Ho atom) (**c**) The 3D supramolecular assembly of **2** viewing along the *b* axis. (red for O atom, and gray-white for Ho and C atoms) (**d**) The 3D supramolecular assembly of **2** viewing along the *c* axis.

Table 4. Bond lengths (Å) and angles (°) around Ho(III) ion in **2** [1].

Ho(1)–O(9)	**2.305(5)**	**Ho(1)–O(6)$_{i}$**	**2.317(6)**
Ho(1)–O(10)	2.327(6)	Ho(1)–O(3)$_{ii}$	2.367(5)
Ho(1)–O(11)	2.375(6)	Ho(1)–O(5)	2.379(6)
Ho(1)–O(1)	2.408(5)	Ho(1)–O(2)$_{iii}$	2.415(5)
O(9)–Ho(1)–O(6)$_{i}$	143.2(2)	O(9)–Ho(1)–O(10)	81.6(2)
O(6)$_{i}$–Ho(1)–O(10)	109.8(2)	O(9)–Ho(1)–O(3)$_{ii}$	74.6(2)
O(6)$_{i}$–Ho(1)–O(3)$_{ii}$	77.4(2)	O(10)–Ho(1)–O(3)$_{ii}$	145.0(2)
O(9)–Ho(1)–O(11)	109.5(2)	O(6)$_{i}$–Ho(1)–O(11)	85.1(2)
O(10)–Ho(1)–O(11)	139.2(3)	O(3)$_{ii}$–Ho(1)–O(11)	74.2(2)
O(9)–Ho(1)–O(5)	142.9(2)	O(6)$_{i}$–Ho(1)–O(5)	72.1(2)
O(10)–Ho(1)–O(5)	72.0(3)	O(3)$_{ii}$–Ho(1)–O(5)	139.7(2)
O(11)–Ho(1)–O(5)	77.5(2)	O(9)–Ho(1)–O(1)	74.4(2)
O(6)$_{i}$–Ho(1)–O(1)	141.6(2)	O(10)–Ho(1)–O(1)	76.8(3)
O(3)$_{ii}$–Ho(1)–O(1)	119.6(2)	O(11)–Ho(1)–O(1)	69.4(2)
O(5)–Ho(1)–O(1)	74.6(2)	O(9)–Ho(1)–O(2)$_{iii}$	76.1(2)
O(6)$_{i}$–Ho(1)–O(2)$_{iii}$	73.6(2)	O(10)–Ho(1)–O(2)$_{iii}$	75.2(2)
O(3)$_{ii}$–Ho(1)–O(2)$_{iii}$	74.3(2)	O(11)–Ho(1)–O(2)$_{iii}$	145.0(2)
O(5)–Ho(1)–O(2)$_{iii}$	119.7(2)	O(1)–Ho(1)–O(2)$_{iii}$	141.6(2)

[1] Symmetry transformations used to generate equivalent atoms: i = $-x+1, -y+1, -z+1$; ii = $x, y+1, z$; iii = $x, -y+1/2, z-1/2$.

Table 5. The O–H···O hydrogen bonds for **2** [1].

D–H···A	**D–H (Å)**	**H···A (Å)**	**D···A (Å)**	**∠ D–H···A (°)**
O(9)–H(9A)···O(4)	0.854(6)	1.869(5)	2.689(8)	160.4(4)
O(9)–H(9B)···O(4)$_{i}$	0.848(6)	1.848(5)	2.696(8)	177.7(4)
O(10)–H(10A)···O(1)$_{ii}$	0.856(6)	1.886(5)	2.668(8)	151.1(4)
O(10)–H(10B)···O(7)$_{iii}$	0.856(6)	2.011(5)	2.774(5)	147.9(4)
O(10)–H(10B)···O(8)	0.856(6)	2.026(5)	2.678(5)	132.2(4)
O(11)–H(11A)···O(2)$_{iv}$	0.857(6)	1.918(5)	2.746(5)	162.1(4)
O(11)–H(11B)···O(4)$_{v}$	0.853(6)	2.181(5)	2.941(5)	148.1(4)

[1] Symmetry transformations used to generate equivalent atoms: i = $-x+2, -y, -z$; ii = $x, -y+1/2, z-1/2$; iii = $-x+1, y+1/2, -z+3/2$; iv = $x, y+1, z$; v = $x, -y+1/2, z+1/2$.

Compared **1**, **2** and the other Ho(III)-squarate polymeric framework, $[Ho_2(C_4O_4)_3(H_2O)_4]_n$ (**3**), synthesized under solvothermal condition reported in the previous literature [66]. The Ho(III) ions in **1** an **2** are both eight-coordinate, but, in **3**, is nine coordinate with a tricapped trigonal prismatic coordination environment. The inherent character of Ho(III) ion with high affinity for oxygen atoms and high coordination numbers [13–29], result in the formation of Ho(III)-squarate coordination polymers with flexible coordination geometry and various structural dimensionality. The squarate act as bridging ligands with $\mu_{1,2}$-bis-monodentate (Scheme 1b) coordination mode in **1**, $\mu_{1,2,3}$-tris-monodentate (Scheme 1c) and $\mu_{1,2}$-bis-monodentate (Scheme 1b) coordination modes in **2** and bidentate/monodentate μ_3– (Scheme 1g) and bidentate/monodentate μ_4– (Scheme 1i) coordination modes in **3**, connecting the Ho(III) ions forming 1D chain, 2D bi-layer and 2D network structures, respectively. The numbers of oxygen atoms of squarate ligand bonded to the Ho(III) ion in **1**, **2** and **3** are 2, 5 and 5, respectively. The oxalate ligands in **1**, instead of squarate ligands, bonded to the Ho(III) ion in a bis-chelating bridging mode connect two Ho(III)-squarate chain forming a 1D ladder-like polymeric framework, which generate 1D hydrophilic pores for the accumulation of guest water molecules in the 3D supramolecular architecture. It is important to note that both the coordinated and guest water molecules play important roles on the construction of their 3D supramolecular architectures and further stabilized via the intermolecular O−H···O hydrogen bonds among the squarate or oxalate ligands, coordinated and guest water molecules.

3.4. Thermal Stability of CPs **1** and **2**

In order to investigate the thermal stability and structural variation of compounds **1** and **2**, thermogravimetric analysis (TGA) and in-situ temperature dependent XRD measurements were performed as shown in Figures 3 and 4, respectively. During the heating process, the TGA of **1** (Figure 3a) revealed that a two-steps weight-losses were observed with the first weight loss of 24.7% occurred in the range of approximate 47–269 °C, corresponding to the losses of coordinated and solvated water molecules (calc. 25.2%) and then thermal stable up to 375 °C without any weight loss. On further heating, samples decomposed at approximately 375–700 °C. The TGA of **2** (Figure 4a) revealed that **2** is thermally stable up to 95 °C and then a two-step weight-losses were observed with the first weight loss of 17.4% occurred in the range of approximate 95–197 °C, corresponding to the loss of coordinated water molecules (calc. 17.0%) and then thermal stable up to 403 °C without any weight loss. On further heating, these samples decomposed at approximately 403–700 °C. To gain the structural changes as a function of the temperature, in situ powder XRD patterns of **1** and **2** were performed and the results at several specific temperatures were shown in Figures 3b and 4b, respectively. Based on the result of TGA, the guest and coordinated water molecules in **1** are lost in the first-step weight loss. The subtle relative intensity varies between RT data and simulation pattern, it may be due to the composition change of solvated and coordinated water molecules. Above 140 °C, the crystallinity becomes worse and worse. As the temperature rising from 170 °C to 200 °C, the framework structure collapsed. The powder XRD patterns of **2** was shown in Figure 4b. The pattern at RT is almost identical to the simulation one obtained from single-crystal X-ray diffraction data. As the temperature rising to 200 °C, a phase transition occurred and can be sustained at 440 °C. As the temperature above 470 °C, **2** decomposed to an amorphous phase. All of the in-situ PXRD measurements are in agreement with the TGA.

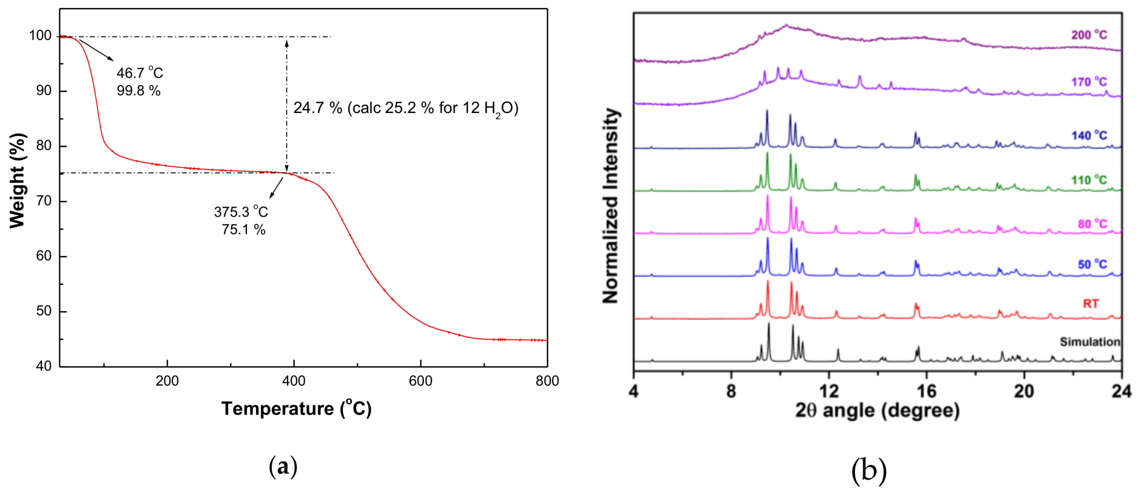

Figure 3. (**a**) Thermogravimetric analysis (TGA) and (**b**) in-situ temperature dependent powder X-ray diffraction (XRD) measurements of **1**.

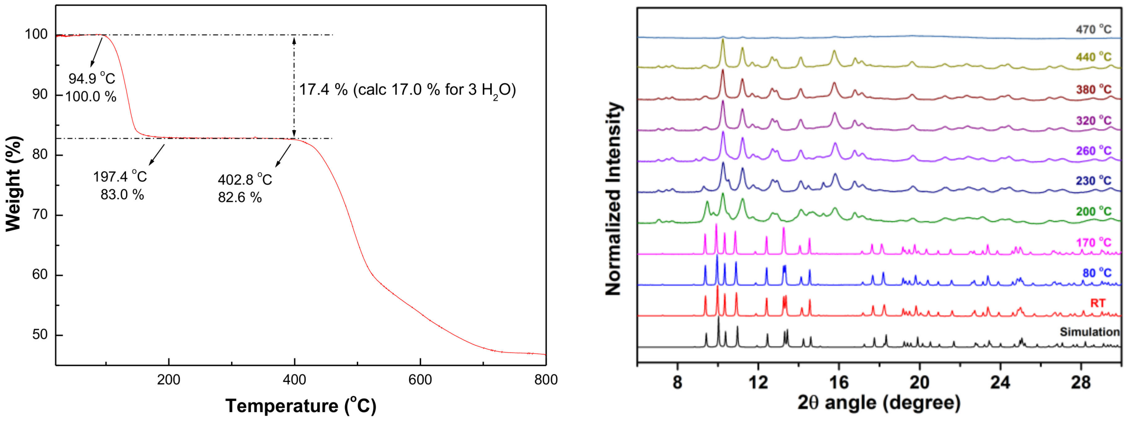

(**a**) (b)

Figure 4. (**a**) TGA and (**b**) in-situ temperature dependent powder XRD measurements of **2**.

*3.5. UV-Visible Spectroscopy of CPs **1** and **2***

The solid-state adsorption spectra of $[Ho(C_2O_4)_{0.5}(C_4O_4)(H_2O)_4]{\cdot}2(H_2O)$ (**1**) and $[Ho(C_4O_4)(H_2O)_3]_n$ (**2**) were investigated at room temperature. As shown in Figure 5, the adsorption spectra bands of $[Ho(C_2O_4)_{0.5}(C_4O_4)(H_2O)_4]{\cdot}2(H_2O)$ (**1**, black line) and $[Ho(C_4O_4)_{1.5}(H_2O)_3]_n$ (**2**, black line) both shows peaks at 361, 386, 418, 451, 468, 474, 486, 537 and 642 nm which can be ascribed to the $(^3H_6, ^5G_5) \leftarrow {}^5I_8$, $^3K_7 \leftarrow {}^5I_8$, $^5G_5 \leftarrow {}^5I_8$, $(^5F_1, ^5G_6) \leftarrow {}^5I_8$, $^3K_8 \leftarrow {}^5I_8$, $^5F_2 \leftarrow {}^5I_8$, $^5F_3 \leftarrow {}^5I_8$, $(^5F_4, ^5S_2) \leftarrow {}^5I_8$ and $^5F_5 \leftarrow {}^5I_8$ transitions of the Ho^{3+} ion, respectively [81,82]. Interestingly, Figure 5a–d) also show reversible color changes immediately and UV-Vis spectra of **1** and **2** under illumination from an incandescent source/daylight to a LED light with a cellphone. The color change between pink (Figure 5a of **1** and Figure 5c of **2** and light yellow (Figure 5b of **1** and Figure 5d of **2** of the Ho^{3+} ion is caused by two absorption bands: $(^5F_1, ^5G_6) \leftarrow {}^5I_8$ and $(^5F_4, ^5S_2) \leftarrow {}^5I_8$. The $^5G_6 \leftarrow {}^5I_8$ transition at 447 nm is a so called "hypersensitive transition," which intensity is dependent on the local surrounding of the holmium ion in symmetry and the ligand type [81]. Accordingly, in comparison to the Figure 5a,c, **1** and **2** have an enhanced adsorption in the region around 450–480 nm (red line in the UV spectra), indicating that the ligand may enhance the absorption of whole coordination polymers.

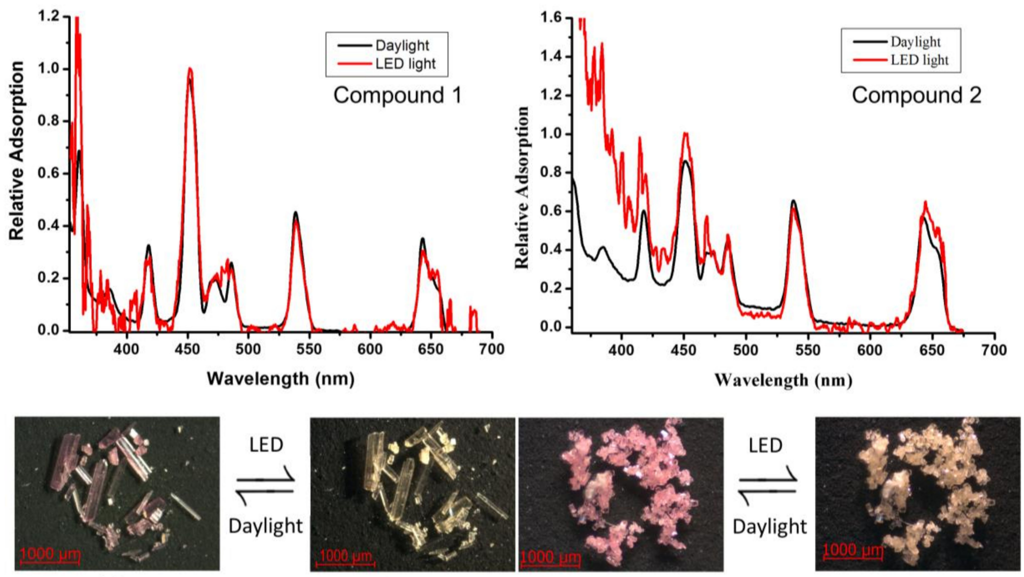

(a) (b) (c) (d)

Figure 5. The color-changing images and UV spectra of **1** (**a**) & (**b**) and **2** (**c**) & (**d**).

4. Conclusions

In conclusion, two 3D supramolecular frameworks, $[Ho_2(C_2O_4)(C_4O_4)_2(H_2O)_8]{\cdot}4(H_2O)$ (**1**) and $[Ho(C_4O_4)_{1.5}(H_2O)_3]$ (**2**), have been successfully synthesized under a facile one-pot synthetic route and their structural versatility of the Ho(III) ion bridged by $C_4O_4^{2-}$ ligands have been studied in detail. The high affinity for oxygen atoms and high coordination numbers of Ho(III) ions result in the formation of eight-coordinate environments bonded to oxygen atoms of two squarate, one oxalate and four water molecules in **1** and five squarate and three water molecules in **2**, respectively. In **1**, both the squarate and oxalate act as bridging ligands adopting $\mu_{1,2}$-*bis*-monodentate and *bis*-chelating coordination modes, respectively, connecting the Ho(III) ions forming the 1D ladder-like CPs, which generates hydrophilic pores intercalated guest water molecules. In **2**, the squarate acts as bridging ligand with two coordination modes, $\mu_{1,2}$-*bis*-monodentate and $\mu_{1,2,3}$-tris-monodentate, connecting the Ho(III) ions forming 2D bi-layered MOFs. Intermolecular hydrogen bonds among the squarate, oxalate ligands and coordinated, guest water molecules provide the main force on the structural extension from their 1D ladder-like CP or 2D layered MOF to 3D supramolecular architectures. The solid-state adsorption spectra of **1** and **2** both show reversible color-changing images under illumination from an incandescent source/daylight to a LED light with a cellphone. Both **1** and **2** have an enhanced adsorption in the region around 450-480 nm (red line in the UV spectra), indicating that the ligand may enhance the absorption of whole coordination polymers.

Author Contributions: C.-C.W. conceived and designed the experiments; S.-Y.K. and Y.F. performed the experimental parts, including synthesis, structural characterization, EA, IR and TGA of compounds; M.-L.H., contributed to measurements of luminescence property and analyzed the data; G.-H.L. contributed to the single-crystal X-ray Data collection and structural analysis of compounds **1** and **2**; C.-K.C. and Y.-C.C. contributed to the powder X-ray diffraction measurements by synchrotron radiation light source; C.-C.W., Y.-C.C. and M.-L.H. wrote the paper.

Funding: This research received no external funding.

Acknowledgments: We appreciate the financial support from the Ministry of Science and Technology and Soochow University of Taiwan.

Conflicts of Interest: The authors declare no conflict of interest.

References

1. Bradshaw, D.; Claridge, J.B.; Cussen, E.J.; Prior, T.J.; Rosseinsky, M.J. Design, Chirality and Flexibility in Nanoporous Molecule-Based Materials. *Acc. Chem. Res.* **2015**, *38*, 273–282. [CrossRef] [PubMed]
2. Kitagawa, S.; Kitaura, R.; Noro, S.I. Functional Porous Coordination Polymers. *Angew. Chem. Int. Ed.* **2004**, *43*, 2334–2375. [CrossRef] [PubMed]
3. Uemura, T.; Horike, S.; Kitagawa, S. Polymerization in Coordination Nanospaces. *Chem. Asian J.* **2006**, *1*, 36–44. [CrossRef] [PubMed]
4. Férey, G. Hybrid Porous Solids: Past, Present, Future. *Chem. Soc. Rev.* **2008**, *37*, 191–214. [CrossRef] [PubMed]
5. Wang, B.; Côté, A.P.; Furukawa, H.; O'Keeffe, M.; Yaghi, O.M. Colossal Cages in Zeolitic Imidazolate Frameworks as Selective Carbon Dioxide reservoirs. *Nature* **2008**, *453*, 207–211. [CrossRef] [PubMed]
6. Rosi, N.L.; Kim, J.; Eddaoudi, M.; Chen, B.L.; O'Keeffe, M.; Yaghi, O.M. Rod Packings and Metal-Organic Frameworks Constructed from Rod-Shaped Secondary Building Units. *J. Am. Chem. Soc.* **2005**, *127*, 1504–1518. [CrossRef] [PubMed]
7. Hayashi, H.; Côté, A.P.; Furukawa, H.; O'keeffe, M.; Yaghi, O.M. Zeolite, A Imidazolate Frameworks. *Nat. Mater.* **2007**, *6*, 501–506. [CrossRef]
8. Thallapally, P.K.; Mcgrail, B.P.; Dalgarno, S.J.; Schaef, H.T.; Tian, J.; Atwood, J.L. Gas-Induced Transformation and Expansion of a Non-Porous Organic Solid. *Nat. Mater.* **2008**, *7*, 146–150. [CrossRef]
9. Banerjee, R.; Phan, A.; Wang, B.; Knobler, C.; Furukawa, H.; O'Keeffe, M.; Yaghi, O.M. High-Throughput Synthesis of Zeolitic Imidazolate Frameworks and Application to CO_2 Capture. *Science* **2008**, *319*, 939–943. [CrossRef]

10. Benelli, C.; Gatteschi, D. Magnetism of Lanthanides in Molecular Materials with Transition-Metal Ions and Organic Radicals. *Chem. Rev.* **2002**, *102*, 2369–2388. [CrossRef]
11. Bünzli, J.C.G.; Piguet, C. Taking Advantage of Luminescent Lanthanide ions. *Chem. Soc. Rev.* **2005**, *34*, 1048–1077. [CrossRef]
12. Chandler, B.D.; Cram, D.T.; Shimizu, G.K.H. Microporous Metal-Organic Frameworks Formed in a Stepwise Manner from Luminescent Building Blocks. *J. Am. Chem. Soc.* **2006**, *128*, 10403–10412. [CrossRef]
13. Wang, P.; Ma, J.P.; Dong, Y.B.; Huang, R.Q. Tunable Luminescent Lanthanide Coordination Polymers Based on Reversible Solid-State Ion-Exchange Monitored by Ion-Dependent Photoinduced Emission Spectra. *J. Am. Chem. Soc.* **2007**, *129*, 10620–10621. [CrossRef]
14. Guo, X.D.; Zhu, G.S.; Fang, Q.R.; Xue, M.; Tian, G.; Sun, J.Y.; Li, X.T.; Qiu, S.L. Synthesis, Structure and Luminescent Properties of Rare Earth Coordination Polymers Constructed from Paddle-Wheel Building Blocks. *Inorg. Chem.* **2005**, *44*, 3850–3855. [CrossRef]
15. Guo, X.D.; Zhu, G.S.; Li, Z.Y.; Chen, Y.; Li, X.T.; Qiu, S.L. Rare Earth Coordination Polymers with Zeolite Topology Constructed from 4-Connected Building Units. *Inorg. Chem.* **2006**, *45*, 4065–4070. [CrossRef]
16. Devic, T.; Serre, C.; Audebrand, N.; Marrot, J.; Férey, G. MIL-103, A 3-D Lanthanide-Based Metal Organic Framework with Large One-Dimensional Tunnels and A High Surface Area. *J. Am. Chem. Soc.* **2005**, *127*, 12788–12789. [CrossRef]
17. Harbuzaru, B.V.; Corma, A.; Rey, F.; Atienzar, P.; Jordá, J.L.; García, H.; Ananias, D.; Carlos, L.D.; Rocha, J. Metal-Organic Nanoporous Structures With Anisotropic Photoluminescence and Magnetic Properties and Their Use as Sensors. *Angew. Chem. Int. Ed.* **2008**, *47*, 1080–1083. [CrossRef]
18. Wang, J.G.; Huang, C.C.; Huang, X.H.; Liu, D.S. Three-Dimensional Lanthanide Thiophenedicarboxylate Framework with an Unprecedented (4,5)-Connected Topology. *Cryst. Growth Des.* **2008**, *8*, 795–798. [CrossRef]
19. Liu, Y.L.; Kravtsov, V.C.; Eddaoudi, M. Template-Directed Assembly of Zeolite-Like Metal-Organic Frameworks (ZMOFs): A Usf-ZMOF with an Unprecedented Zeolite Topology. *Angew. Chem. Int. Ed.* **2008**, *47*, 8446–8449. [CrossRef]
20. Pan, L.; Woodlock, E.B.; Wang, X. A New Porous Three-Dimensional Lanthanide Coordination Polymer. *Inorg. Chem.* **2000**, *39*, 4174–4178. [CrossRef]
21. Lipstman, S.; Muniappan, S.; George, S.; Goldberg, I. Framework Coordination Polymers of Tetra(4-carboxyphenyl)porphyrin and Lanthanide Ions in Crystalline Solids. *Dalton Trans.* **2007**, *30*, 3273–3281. [CrossRef]
22. Muniappan, S.; Lipstman, S.; George, S.; Goldberg, I. Porphyrin Framework Solids. Synthesis and Structure of Hybrid Coordination Polymers of Tetra(carboxyphenyl)porphyrins and Lanthanide-Bridging Ions. *Inorg. Chem.* **2007**, *46*, 5544–5554. [CrossRef]
23. He, Y.; Furukawa, H.; Wu, C.; O'Keeffe, M.; Chen, B. A Mesoporous Lanthanide-Organic Framework Constructed from a Dendritic Hexacarboxylate with Cages of 2.4 nm†. *CrystEngComm* **2013**, *15*, 9328–9331. [CrossRef]
24. He, Y.; Furukawa, H.; Wu, C.; O'Keeffe, M.; Krishna, R.; Chen, B. Low-energy regeneration and high productivity in a lanthanide–hexacarboxylate framework for high-pressure CO_2–CH_4–H_2 separation. *Chem. Commun.* **2013**, *49*, 6773–6775. [CrossRef]
25. He, H.Y.; Ma, H.Q.; Sun, D.; Zhang, L.L.; Wang, R.M.; Sun, D.F. Porous Lanthanide-Organic Frameworks: Control over Interpenetration, Gas Adsorption and Catalyst Properties. *Cryst. Growth Des.* **2013**, *13*, 3154–3161. [CrossRef]
26. Mihalcik, D.J.; Zhang, T.; Ma, L.; Lin, W. Highly Porous 4,8-Connected Metal-Organic Frameworks: Synthesis, Characterization and Hydrogen Uptake. *Inorg. Chem.* **2012**, *51*, 2503–2508. [CrossRef]
27. Decadt, R.; Van Hecke, K.; Depla, D.; Leus, K.; Weinberger, D.; Van Driessche, I.; Van Der Voort, P.; Van Deun, R. Synthesis, Crystal Structures and Luminescence Properties of Carboxylate Based Rare-Earth Coordination Polymers. *Inorg. Chem.* **2012**, *51*, 11623–11634. [CrossRef]
28. Yan, L.; Yue, Q.; Jia, Q.X.; Lemercier, G.; Gao, E.Q. Lanthanide Metal-Organic Frameworks Based on Octahedral Secondary Building Units: Rare Net Topology and Luminescence. *Cryst. Growth Des.* **2009**, *9*, 2984–2987. [CrossRef]

29. Yang, J.; Yue, Q.; Li, G.D.; Cao, J.J.; Li, G.H.; Chen, J.S. Structures, Photoluminescence, Up-Conversion and Magnetism of 2D and 3D Rare-Earth Coordination Polymers with Multicarboxylate Linkages. *Inorg. Chem.* **2006**, *45*, 2857–2865. [CrossRef]
30. Khan, M.I.; Chang, Y.D.; Chen, Q.; Salta, J.; Lee, Y.S.; O'Connor, C.J.; Zubieta, J. Synthesis and Characterization of Binuclear Oxo-Vanadium Complexes of Carbon Oxoanion Ligands. Crystal Structures of the Binuclear Vanadium(IV) Complex $(NH_4)[V_2O_2(OH)(C_4O_4)_2(H_2O)_3]$.cntdot.$H_2O$, of the Mixed-Valence Vanadium(V)/Vanadium(IV)-Squarate Species $[(n\text{-}C_4H_9)_4N]$ $[V_2O_3(C_4O_4)_2(H_2O)_3]$.cntdot.$3H_2O$ and $[(C_4H_9)_4N]_4[V_4O_6(C_4O_4)_5(H_2O)_4]$. cntdot. $6H_2O$ and of the Binuclear Vanadium(IV)-Oxalate Species $[V_2O_2Cl_2(C_2O_4)(CH_3OH)_4]$.cntdot.$2Ph_4PCl$. *Inorg. Chem.* **1994**, *33*, 6340–6350.
31. Lee, C.R.; Wang, C.C.; Wang, Y. Structural Relationship of Various Squarates. *Acta. Cryst.* **1996**, *52*, 966–975. [CrossRef]
32. Trombe, J.C.; Petit, J.-F.; Gleizes, A. Lanthanide Oxalato-Squarates-Preparation and Crystal-Structures of (CE_2 (H_2O) 8 (C_4O_4) 2 (C_2O_4)). $3H_2O$ and EU_2 (H_2O) 4 (C_4O_4) 2 (C_2O_4). *Eur. J. Solid State Inorg. Chem.* **1991**, *28*, 669–681.
33. Trombe, J.C.; Sabadie, L.; Millet, P. Synthesis and Crystal Structure of $La(H_2O)(C_2O_4)_2\cdot(CN_3H_6)$ and of $[Nd(H_2O)]_2(C_2O_4)_4\cdot(NH_4)(CN_3H_6)$. *Solid State Sci.* **2002**, *4*, 1199–1208.
34. Soules, R.; Dahan, F.J.; Laurent, P.; Castan, P. A Novel Co-Ordination Mode for the Squarate Ligand [Dihydroxycyclobutenedionate(2–)]: Synthesis, Crystal Structure and Magnetic Properties of Catena-Diaqua(2,2′-Bipyridyl)-μ-(Squarato- O^1, O^2)-Nickel(II) Dihydrate. *J. Chem. Soc. Dalton Trans.* **1988**, *3*, 587–590. [CrossRef]
35. Hall, L.A.; Williams, D.J.; Menzer, S.; White, A.J.P. The Complexing Properties of 1-Aminosquarate Derivatives with Lead. *Inorg. Chem.* **1997**, *36*, 3096–3101. [CrossRef]
36. Alleyne, B.D.; Hall, L.A.; Hosein, H.A.; Jaggernauth, H.; White, A.J.P.; Williams, D.J. Hydrogen-Bonding Interactions in the Deries of Complexes $[M(C_4O_4)(OH_2)_2(dmf)_2]$ and $[M(C_4O_4)(OH_2)_4]$ (M = Mn, Co, Ni, Cu, Zn). *J. Chem. Soc. Dalton Trans.* **1998**, *22*, 3845–3850. [CrossRef]
37. Lai, S.F.; Cheng, C.Y.; Lin, K. Hydrothermal Synthesis of a Thermally Stable Poroussupramolecular π–π Framework:$[\{Co_2(C_{12}H_8N_2)_4(\mu\text{-}C_4O_4)(OH_2)_2\}C_4O_4]\cdot 8H_2O$. *J. Chem. Commun.* **2001**, 1082–1083. [CrossRef]
38. Grove, H.; Sletten, J.; Julve, M.; Lloret, F.; Cano, J. Syntheses, Crystal Structures and Magnetic Properties of One- and Two-Dimensional Pap-Containing Copper(II) Complexes (Pap = Pyrazino[2–f][4,7]Phenanthroline). *J. Chem. Soc. Dalton Trans.* **2001**, *3*, 259–265. [CrossRef]
39. Nather, C.; Greve, J.; Jess, I. New Coordination Polymer Changing Its Color upon Reversible Deintercalation and Reintercalation of Water: Synthesis, Structure and Properties of Poly[Diaqua-(μ_2-Squarato-O,O′)-(μ_2-4,4′-Bipyridine-N,N′)- Manganese(II)] Trihydrate. *Chem. Mater.* **2002**, *14*, 4536–4542. [CrossRef]
40. Piggott, P.M.T.; Hall, L.A.; White, A.J.P.; Williams, D.J. Attempted Syntheses of Lanthanide(III) Complexes of the Anisole- and Anilinosquarate Ligands. *Inorg. Chem.* **2003**, *42*, 8344–8352. [CrossRef]
41. Yang, B.P.; Mao, J.G. New Types of Metal Squarato-phosphonates: Condensation of Aminodiphosphonate with Squaric Acid under Hydrothermal Conditions. *Inorg. Chem.* **2005**, *44*, 566–571. [CrossRef]
42. Konar, S.; Corbella, M.; Zangrando, E.; Ribas, J.; Chaudhuri, N.R. The First Unequivocally Ferromagnetically Coupled Squarato Complex: Origin of the Ferromagnetism in an Interlocked 3D Fe(II) System. *Chem. Commun.* **2003**, *12*, 1424–1425. [CrossRef]
43. Ghosh, A.K.; Ghoshal, D.; Zangrando, E.; Ribas, J.; Chaudhuri, N.R. Structural Diversity in Manganese Squarate Frameworks Using N,N-Donor Chelating/Bridging Ligands: Syntheses, Crystal Structures and Magnetic Properties. *Dalton Trans.* **2006**, *12*, 1554–1563. [CrossRef]
44. Chen, Q.; Liu, S.; Zubieta, J. Coordination Chemistry of Polyoxomolybdates: The Structure of a Dodecanuclear Molybdate Cage Incorporating Hydrogen Squarate Ligands, $[(C_4H_9)_4N]_4$ $[Mo_{12}O_{36}(C_4O_4H)_4]\cdot 10Et_2O$. *Angew Chem. Int. Ed.* **1990**, *29*, 70–72. [CrossRef]
45. Lin, K.J.; Lii, K.H. Binuclear Vanadium(III) Squarates with Layered and Framework Structures: Hydrothermal Synthesis and Structures of $[\{V(OH)(C_4O_4)(H_2O)\}_2]$ and $[\{V(OH)(C_4O_4)\}_2]\cdot 4H_2O$. *Angew. Chem. Int. Ed. Engl.* **1997**, *36*, 2076–2077. [CrossRef]
46. Hosein, H.A.; Hall, L.A.; Lough, A.J.; Desmarais, W.; Vela, M.J.; Foxman, B.M. Attempted Syntheses of Transition Metal and Lanthanide (Dialkylamino)squarates. The Hydrolysis Problem. *Inorg. Chem.* **1998**, *37*, 4184–4189. [CrossRef]

47. Hosein, H.A.; Jaggernauth, H.; Alleyne, B.D.; Hall, L.A.; White, A.J.P.; Williams, D.J. First-Row Transition-Metal Complexes of the 1-Methoxycyclobutenedionate(1−) Ion. *Inorg. Chem.* **1999**, *38*, 3716–3720. [CrossRef]
48. Spandl, J.; Brüdgam, I.; Hartl, H. Solvothermal Synthesis of a 24-Nuclear, Cube-Shaped Squarato-oxovanadium (IV) Framework: $[N(nBu)_4]_8[V_{24}O_{24}(C_4O_4)_{12}(OCH_3)_{32}]$. *Angew. Chem. Int. Ed. Engl.* **2001**, *40*, 4018–4020. [CrossRef]
49. Maji, T.K.; Mostafa, G.; Sain, S.; Prasad, J.S.; Chaudhuri, N.R. Construction of a 3D Array of Cadmium(II) Using Squarate as a Building Block. *CrystEngComm* **2001**, *3*, 155–158. [CrossRef]
50. Mukherjee, P.S.; Konar, S.; Zangrando, E.; Diaz, C.; Chaudhuri, N.R. Synthesis, Crystal Structure and Magneto-Structural Correlation of Two Bi-Bridging 1D Copper(II) Chains. *J. Chem. Soc. Dalton Trans.* **2002**, *18*, 3471–3476. [CrossRef]
51. Neeraj, S.; Noy, M.L.; Rao, C.N.R.; Cheetham, A.K. Sodalite Networks Formed by Metal Squarates. *Solid State Sci.* **2002**, *4*, 1231–1236. [CrossRef]
52. Dan, M.; Rao, C.N.R. An Open-Framework Cobalt Oxalato-Squarate Containing a Ligated Amine. *Solid State Sci.* **2003**, *5*, 615–620. [CrossRef]
53. Kurmoo, M.; Kumagai, H.; Chapman, K.W.; Kepert, C.J. Reversible Ferromagnetic-Antiferromagnetic Transformation Upon Dehydration-Hydration of the Nanoporous Coordination Framework, $[Co_3(OH)_2(C_4O_4)_2]·3H_2O$. *Chem. Commun.* **2005**, 3012–3014. [CrossRef]
54. Gandara, F.; Gomez-Lor, B.; Iglesias, M.; Snejko, N.; Gutierrez-Puebla, E. A New Scandium Metal Organic Framework Built up from Octadecasil Zeolitic Cages as Heterogeneous Catalyst. *Chem. Commun.* **2009**, 2393–2395. [CrossRef]
55. Gutschke, S.O.H.; Molinier, M.; Powell, A.K.; Wood, P.T. Hydrothermal Synthesis of Microporous Transition Metal Squarates: Preparation and Structure of $[CO_3(\mu_3\text{-}OH)_2(C_4O_4)_2]·3H_2O$. *Angew. Chem. Int. Ed. Engl.* **1997**, *36*, 991–992. [CrossRef]
56. Yufit, D.S.; Price, D.J.; Howard, J.A.K.; Gutschke, S.O.H.; Powell, A.K.; Wood, P.T. New Type of Metal Squarates. Magnetic and Multi-Temperature X-ray Study of Di-Hydroxy(μ6-squarato)manganese†. *Chem. Commun.* **1999**, *16*, 1561–1562. [CrossRef]
57. Trombe, J.C.; Sabadie, L.; Millet, P. Hydrothermal Synthesis and Structural Characterization of Fe(II)-squarate $Fe_2(OH)_2(C_4O_4)$. *Solid State Sci.* **2002**, *4*, 1209–1212. [CrossRef]
58. Yang, C.H.; Chou, C.M.; Lee, G.H.; Wang, C.C. Self-Assembly of Two Mixed-Ligands Metal-Organic Coordination Polymers,$[MII_2\ (DPA)_2(C_4O_4)(C_2O_4)]$(M= Cu, Zn). *Inorg. Chem. Commun.* **2003**, *6*, 135–140. [CrossRef]
59. Wang, C.C.; Yang, C.H.; Tseng, S.M.; Lee, G.H.; Sheu, H.S.; Phyu, K.W. A New Moisture-Sensitive Metal-Coordination Solids $\{[Cd(C_4O_4)(bipy)(H_2O)_2]\ 3H_2O\}\infty$ (bipy = 4,4′-bipyridine). *Inorg. Chim. Acta* **2004**, *357*, 3759–3764. [CrossRef]
60. Wang, C.C.; Yang, C.H.; Lee, G.H.; Tsai, H.L. Syntheses, Structures and Magnetic Properties of Two 1D, Mixed-Ligand,Metal Coordination Polymers, $[M(C_4O_4)(dpa)(OH_2)]$ (M = CoII, NiII and ZnII; dpa = 2,2′-dipyridylamine) and $[Cu(C_4O_4)(dpa)(H_2O)]2·(H_2O)$. *Eur. J. Inorg. Chem.* **2005**, *7*, 1334–1342. [CrossRef]
61. Wang, C.C.; Yang, C.H.; Lee, G.H. Hydrothermal Synthesis and Structural Characterization of Two pH-Controlled Cd–Squarate Coordination Frameworks, $[Cd_2(C_4O_4)2.5(H_2O)_4]·(dpaH)·1.5(H_2O)$ and $[Cd(C_4O_4)(dpa)(OH_2)]$ (dpa = 2,2′-dipyridylamine). *Eur. J. Inorg. Chem.* **2006**, *4*, 820–826. [CrossRef]
62. Wang, C.C.; Tseng, S.M.; Lin, S.Y.; Liu, F.C.; Dai, S.C.; Lee, G.H.; Shih, W.J.; Sheu, H.S. Assemblies of Two Mixed-Ligand Coordination Polymers with Two-Dimensional Metal-Organic Frameworks Constructed from M(II) Ions with Croconate and 1,2-Bis-(4-pyridyl)ethylene (M = Cd and Zn). *Cryst. Growth Des.* **2007**, *7*, 1783–1790. [CrossRef]
63. Wang, C.C.; Ke, S.Y.; Chen, K.T.; Hsieh, Y.F.; Wang, T.H.; Lee, G.H.; Chuang, Y.C. Reversible Single-Crystal-to-Single-Crystal Structural Transformation in a Mixed-Ligand 2D Layered Metal-Organic Framework: Structural Characterization and Sorption Study. *Crystals* **2017**, *7*, 364. [CrossRef]
64. Lin, X.Y.; Zhao, L.M.; Wang, D.H.; Wang, Y.K.; Li, M.; Li, H.H.; Chen, Z.R. Structural Diversities of Squarate-Based Complexes: Photocurrent Responses and Thermochromic Behaviours Enhanced by Viologens. *Inorg. Chem. Front.* **2018**, *5*, 189–199. [CrossRef]
65. Liu, C.M.; Xiang, D.Z.; Hao, X.; Zhu, D.B. Field-Induced Relaxation of Magnetization in a Three-Dimensional LnMOF with the Second Bridging Ligand Squarate. *ACS Omega* **2016**, *1*, 286–292. [CrossRef]

66. Wang, L.; Gu, W.; Deng, X.J.; Zeng, L.F.; Liao, S.Y.; Zhang, M.; Yang, L.Y.; Liu, X. A Series of 2D and 3D Novel Lanthanide Complexes Constructed from Squarate $C_4O_4^{2-}$: Syntheses, Structures, Magnetic Properties and Near-infrared Emission Properties. *Aust. J. Chem.* **2011**, *64*, 1373–1382. [CrossRef]
67. Wang, C.M.; Lii, K.H. Synthesis of Novel Organic-Inorganic Hybrid Compounds: Lanthanide Phosphites Incorporating a Squarate Ligand. *Inorg. Chem.* **2009**, *48*, 6335–6337. [CrossRef]
68. Akkari, H.; Bénard-Rocherullé, P.; Mérazig, H.; Roisnel, T.; Rocherullé, J. Hydrothermal Synthesis, Crystal Structure and Thermal Behavior of the First Lanthanide Sulfato-Squarate, $La_2(H_2O)_4(SO_4)_2(C_4O_4)$. *Solid State Sci.* **2006**, *8*, 704–715. [CrossRef]
69. Mahé, N.; Bataille, T. Synthesis, Crystal Structure from Single-Crystal and Powder X-ray Diffraction Data and Thermal Behavior of Mixed Potassium Lanthanide Squarates: Thermal Transformations of layered $[Ln(H_2O)_6]K(H_2C_4O_4)(C_4O_4)_2$ into Pillared $LnK(C_4O_4)_2$ (Ln = Y, La, Gd, Er). *Inorg. Chem.* **2004**, *43*, 8379–8386. [CrossRef]
70. Heinl, U.; Hinse, P.; Mattes, R. Oxalato- and Quadratato-Komplexe Hochkoordinierter Metallionen: Die Raumnetzstrukturten von $La_2(C_2O_4)(C_4O_4)(H_2O)_8{\cdot}2{,}5H_2O$ und $K[Bi(C_2O_4)_2{\cdot}5H_2O$. *Z. Anorg. Allg. Chem.* **2001**, *627*, 2173–2177. [CrossRef]
71. *SMART V 4 043 Software for CCD Detector System*; Siemens Analytical Instruments Division: Madison, WI, USA, 1995.
72. *SAINT V 4 035 Software for CCD Detector System*; Siemens Analytical Instruments Division: Madison, WI, USA, 1995.
73. Sheldrick, G.M. Program for the Refinement of Crystal Structures. *Shelxl97* **1997**.
74. *SHELXTL 5 03 (PC-Version), Program Liberary for Structure Solution and Molecular Graphics*; Siemens Analytical Instruments Division: Madison, WI, USA, 1995.
75. Toby, B.H.; Von Dreele, R.B. GSAS-II: The Genesis of a Modern Open-Source All Purpose Crystallography Software Package. *J. Appl. Crystallogr.* **2013**, *46*, 544–549. [CrossRef]
76. Chen, Y.T.; Lin, C.Y.; Lee, G.H.; Ho, M.L. Four New Lead(II)–Iridium(III) Heterobimetallic Coordination Frameworks: Synthesis, Structures, Luminescence and Oxygen-Sensing Properties. *CrystEngComm* **2015**, *17*, 2129–2140. [CrossRef]
77. Fabre, P.L.; Castan, P.; Deguenon, D.; Paillous, N. A Photo-Oxidation of Croconic Acid into Oxalic Acid. *Can. J. Chem.* **1995**, *73*, 1298–1304. [CrossRef]
78. Reinoso, S.; Vitoria, P.; Felices, L.S.; Montero, A.; Lezama, L.; Gutirrez-Zorrilla, M.M. NEXTTetrahydroxy-p-benzoquinone as a Source of Polydentate O-Donor Ligands. Synthesis, Crystal Structure and Magnetic Properties of the $[Cu(bpy)(dhmal)]_2$ Dimer and the Two-Dimensional $[\{SiW_{12}O_{40}\}\{Cu_2(bpy)_2(H_2O)(ox)\}_2]{\cdot}16H_2O$ Inorganic-Metalorganic Hybrid. *Inorg. Chem.* **2007**, *46*, 1237–1249. [CrossRef]
79. Ke, S.Y.; Yeh, C.T.; Wang, C.C.; Lee, G.H.; Hwo-Shuenn, S. A 3d-4f Complex Constructed by the Assembly of a Cationic Template, $[Cu(en)_2]^{2+}$ and a 3D Anionic Coordination Polymer, $[Sm_2(C_2O_4)_3(C_5O_5)(H_2O)_2]^{2-}$. *Z. Anorg. Allg. Chem.* **2017**, *643*, 657–663. [CrossRef]
80. Ito, M.; West, R. New Aromatic Anions. IV. Vibrational Spectra and Force Constants for $C_4O_4^{-2}$ and $C_5O_5^{-2}$. *J. Am. Chem. Soc.* **1963**, *85*, 2580–2584. [CrossRef]
81. Binnemans, K.; Görller-Walrand, C. On the Color of the Trivalent Lanthanide Ions. *Chem. Phys. Lett.* **1995**, *235*, 163–174. [CrossRef]
82. Marques, L.F.; Correa, C.C.; Ribeiro, S.J.L.; dos Santos, M.V.; Dutra, J.D.L.; Freire, R.O.; Machado, F.C. Synthesis, Structural Characterization, Luminescent Properties and Theoretical Study of Three Novel Lanthanide Metal-Organic Frameworks of Ho(III), Gd(III) and Eu(III) with 2,5-Thiophenedicarboxylate Anion. *J. Solid State Chem.* **2015**, *27*, 68–78. [CrossRef]